Effects of humidity on aerosols in southern Africa during the biomass burning season

Brian I. Magi and Peter V. Hobbs

Department of Atmospheric Sciences, University of Washington, Seattle, Washington, USA

Received 28 January 2002; revised 21 June 2002; accepted 23 June 2002; published 3 April 2003.

[1] Measurements of the aerosol total light scattering coefficient, σ_{sp}, and the aerosol hemispheric backscatter ratio, $\beta(1)$, as functions of relative humidity (RH in %) (so-called humidographs) at three wavelengths (450, 550, and 700 nm) were obtained in the dry season in southern Africa (1) in ambient air in South Africa, Botswana, Mozambique and Zambia, (2) at various distances downwind in identifiable smoke plumes from biomass fires, and (3) along the southwest coast of Africa. The ratio of σ_{sp} at an RH of 80% to that at 30% provides a measure of the effects of RH on σ_{sp}, and similarly for $\beta(1)$. For the three broad sampling categories given above, and at a wavelength of 550 nm, these ratios varied from 1.42 ± 0.05 to 2.07 ± 0.03 for σ_{sp}, and from 0.69 ± 0.05 to 0.99 ± 0.14 for $\beta(1)$. In general, humidographs for the ambient air samples showed a greater dependence on RH than those for smoke from identifiable biomass fires. During a period when dense, aged smoke was transported to the region from the north, the humidographs for σ_{sp} for ambient air samples were similar to those for identifiable smoke plume samples just ~10- to 50-min old. This suggests that as far as the effects of RH on σ_{sp} are concerned the effects of aging of smoke and its mixing with ambient air are realized within less than about an hour. *INDEX TERMS:* 0305 Atmospheric Composition and Structure: Aerosols and particles (0345, 4801); 0315 Atmospheric Composition and Structure: Biosphere/atmosphere interactions; 0320 Atmospheric Composition and Structure: Cloud physics and chemistry; 0368 Atmospheric Composition and Structure: Troposphere—constituent transport and chemistry; *KEYWORDS:* aerosols, particles, biomass burning, Africa

Citation: Magi, B. I., and P. V. Hobbs, Effects of humidity on aerosols in southern Africa during the biomass burning season, *J. Geophys. Res.*, *108*(D13), 8495, doi:10.1029/2002JD002144, 2003.

1. Introduction

[2] The amount of solar radiation scattered by atmospheric aerosols, and therefore aerosol radiative forcing, depends, among other things, on the ambient relative humidity [e.g., *Pilinis et al.*, 1995; *Kotchenruther and Hobbs*, 1998]. As part of the Southern African Regional Science Initiative 2000 (SAFARI 2000) to characterize atmospheric aerosols in southern Africa during the biomass burning season, the University of Washington's (UW) Cloud and Aerosol Research Group obtained measurements, aboard its Convair-580 research aircraft, of the physical, chemical, and optical properties of aerosol in southern Africa from 10 August to 18 September 2000 (Appendix by P. V. Hobbs in the work of *Sinha et al.* [2003]). In this paper, we describe the effects of relative humidity (RH in %) on the aerosol total light scattering coefficient and the aerosol backscatter ratio as functions of RH and wavelength for various aerosol types encountered in SAFARI 2000.

2. Scope of Measurements

[3] A total of 54 useable plots of light scattering versus RH (called ''humidographs'') were obtained in South Africa, Mozambique, Botswana, Zambia, and Namibia (Figure 1). A humidograph shows the change in the aerosol total light scattering coefficient, or the aerosol hemispheric backscatter ratio, with increasing RH at a specified wavelength (450, 550, or 750 nm for our measurements).

[4] The humidographs obtained in SAFARI 2000 were divided into three broad categories: (1) ambient air samples in South Africa, Botswana, Mozambique and Zambia affected in varying degrees by biomass burning sources but not in identifiable smoke plumes (41 samples); (2) samples from individual smoke plumes from biomass fires (9 samples); (3) ambient air samples in Namibia (4 samples). Table 1 lists the locations, times, and information on the airflows, for all the humidographs.

3. Method of Measurements

[5] To obtain a humidograph for a particular aerosol sample, air was passed through the preheater-humidifier-nephelometer system described by *Kotchenruther and Hobbs* [1998]. The preheater dried the aerosol and the humidifier then steadily increased the RH from ~25% to 85% over a period of about 5 min. During the period of increasing RH, the aerosol total light scattering coefficient

0148-0227/03/2002JD002144$09.00

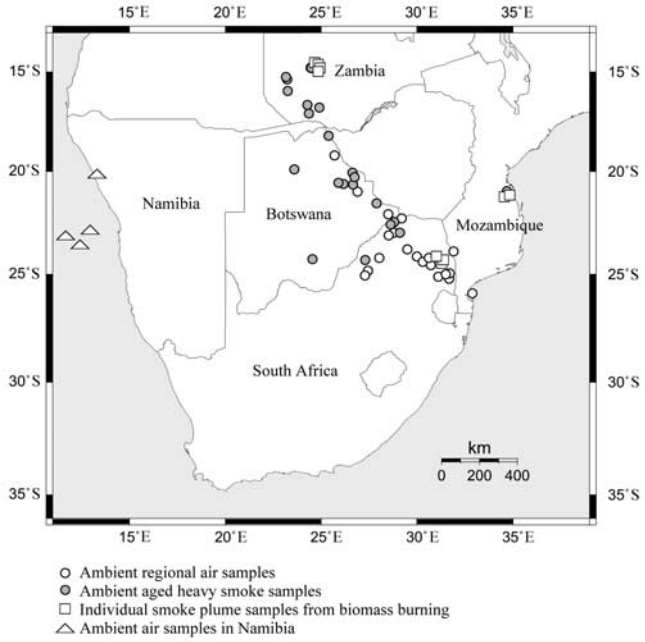

Figure 1. Map of southern Africa showing locations where humidographs were obtained.

and the aerosol hemispheric backscatter coefficient were measured continuously at wavelengths of 450, 550, and 700 nm with a nephelometer (custom-built for the UW by MS Electron). The nephelometer integrated over scattering angles from ~7° to 170° for the total scattering coefficient, and from ~90° to 170° for the hemispheric backscatter coefficient. Corrections for forward and backward angular truncation and for the nonisotropic light source were applied to the nephelometer measurements, using the methods described by *Hartley et al.* [2000] and *Hartley and Hobbs* [2001].

[6] For ambient aerosols, sampling was done by routing outside air continuously into the aircraft through a 5-cm-diameter stainless steel tube that removed aerosol particles larger than ~5-μm diameter. The ambient air was simultaneously monitored by another nephelometer to record any significant changes in the ambient aerosol over the time taken to obtain a humidograph. Humidographs obtained during periods when the ambient aerosol was changing rapidly generally showed large deviations from the empirically determined best fit function (see section 4.1). These humidographs were excluded from this study.

[7] Since the aircraft generally did not reside in an individual smoke plume for the 5 min required to complete a humidograph, smoke plumes were sampled using a different technique. In this case, a sample of smoke from the plume was collected in a 2.5-m^3 Velostat grab bag in ~20 s. This air was then passed through the preheater-humidifier-nephelometer system to obtain a humidograph. Minor particle losses to the surface of the Velostat bag were monitored by an independent nephelometer and the correction method described by *Kotchenruther and Hobbs* [1998] was applied.

[8] Additional information on the sampling procedures used aboard the Convair-580 is given by *Sinha et al.* [2003, Appendix] and *Hobbs et al.* [2003].

4. Analysis of Data

4.1. Empirical Fitting Functions to Humidographs

[9] Various empirical relationships have been used to describe the functional dependence of the aerosol total light scattering coefficient on RH [e.g., *Kasten*, 1969]. *Kotchenruther et al.* [1999] found that the empirical function that provides the best fit to a humidograph depends on whether the aerosol exhibits hygroscopic growth or deliquescent growth. In the present study, both the ambient aerosols and the aerosols in individual smoke plumes from biomass burning exhibited characteristic hygroscopic growth. That is, the aerosol total light scattering coefficient, σ_{sp}, increased with RH without any marked discontinuity. In this case, the RH dependence of σ_{sp} can be fitted to an empirical function of the form

$$\sigma_{sp} = \sigma_{spd}\left[1 + a(RH/100)^b\right] \quad (1)$$

where σ_{spd} is the light scattering coefficient for the dry aerosol, and a and b are empirical fitting parameters. *Hegg et al.* [1996] used a simpler function to describe the hygroscopic growth of marine aerosols, but Kotchenruther and Hobbs showed that equation (1) best described the hygroscopic growth of aerosols from biomass burning in Brazil. The measurements contained in a humidograph were fitted to (1) using a Levenberg-Marquard nonlinear least squares optimization routine. A measure of the dispersion of the fit to each humidograph was determined by the reduced chi-square (χ_r^2) parameter [*Bevington and Robinson*, 1992]. Nineteen humidographs with $\chi_r^2 > 40$ were excluded from this study.

[10] The amount of radiation scattered by an aerosol to the back hemisphere can be quantified by the hemispheric backscatter ratio, $\beta(1)$, which is defined as the ratio of the aerosol hemispheric backscatter coefficient to the aerosol total scattering coefficient [*Wiscombe and Grams*, 1976]. Since $\beta(1)$ decreased approximately linearly with increasing RH, the functional relationship

$$\beta(1) = c\left(\frac{RH}{100}\right) + d \quad (2)$$

was used to fit the measurements, where c and d are fitting parameters.

[11] Direct radiative forcing by aerosols is dependent on the amount of incoming solar radiation that is scattered back to space by the aerosols. *Wiscombe and Grams* [1976] describe how the upscatter fraction can be derived from $\beta(1)$.

4.2. Humidification Factors

[12] We define the humidification factor as the ratio of the aerosol total light scattering coefficient σ_{sp} at an RH of 80% to σ_{sp} at an RH of 30% (where the aerosol is essentially dry). Hence, the humidification factor at a wavelength λ is

$$f(80\%, \lambda) \equiv \frac{\sigma_{sp}(80\%, \lambda)}{\sigma_{sp}(30\%, \lambda)} \quad (3)$$

where σ_{sp} is determined from (1) using the data provided by a humidograph of σ_{sp} versus RH. The corresponding humidification factor for $\beta(1)$ is

$$f_{\beta(1)}(80\%, \lambda) \equiv \frac{\beta(1)(80\%, \lambda)}{\beta(1)(30\%, \lambda)} \quad (4)$$

Table 1. Information on Humidographs Obtained Aboard the University of Washington's Convair-580 Aircraft in SAFARI 2000

Date (2000)	UW Flight Number	Time of Measurement,[a] UTC, hhmm	Latitude, °S	Longitude, °E	Altitude, m, MSL	Synoptic Airflow From	Path of 72-Hour Back Trajectory[b]
(a) Ambient Air Samples Obtained in South Africa, Botswana, Mozambique and Zambia							
14 Aug.	1812	1312	24.82	27.44	2328	S/SE	C
14 Aug.	1812	1337	25.06	27.28	2330	S/SE	C
15 Aug.	1814	0912	25.11	31.11	880	S	M/C
17 Aug.	1815	0826	25.22	31.71	1242	SE/N	M/C
20 Aug.	1819	1151	24.22	28.06	3477	W	C
22 Aug.	1820	0721	24.15	29.99	3057	W	C
22 Aug.	1820	0951	24.95	31.70	884	E/NE	M/C
23 Aug.	1821	1227	23.80	29.50	2945	S	C
24 Aug.	1822	0709	24.40	30.30	3546	W/SW	C
24 Aug.	1822	0945	25.90	32.88	2066	W/S	M/C
29 Aug.	1823	0858	22.80	28.80	2897	S	C
29 Aug.	1823	0928	22.30	29.20	2876	S	C
29 Aug.	1823	1005	23.00	28.80	1603	E	C
29 Aug.	1824	1317	24.55	30.73	3485	SW	C
29 Aug.	1824	1337	25.00	31.50	968	E	C
31 Aug.	1825	0932	23.90	31.90	2953	SW	C
31 Aug.	1825	1108	21.10	34.80	1125	S/N	M/C
1 Sept.	1826	0612	22.10	28.50	3830	SE	C
1 Sept.	1826	0718	19.20	25.70	3237	E/N	C
1 Sept.	1826	0802	16.80	24.90	1896	NE	C
2 Sept.	1829	0852	21.00	26.90	3169	W/NE	C
2 Sept.	1829	1019	19.90	23.60	1581	NE	C
3 Sept.	1830	0733	22.50	28.80	3150	N/NW	C
3 Sept.	1830	0843	20.60	26.16	1106	NE/N	C
3 Sept.	1830	1021	20.55	25.90	2524	NE/N	C
3 Sept.	1830	1058	20.65	26.67	2389	N	C
3 Sept.	1830	1124	21.57	27.89	2376	N	C
5 Sept.	1831	0910	22.48	28.81	3181	N	C
5 Sept.	1831	1005	20.05	26.63	3584	NW/N	C
5 Sept.	1831	1040	18.23	25.39	4226	N	C
5 Sept.	1831	1245	14.71	24.53	1639	N	C
6 Sept.	1832	0728	17.10	24.36	3861	NE	C
6 Sept.	1832	0755	15.92	23.25	1224	NE	C
6 Sept.	1832	0911	15.38	23.22	1240	NE	C
6 Sept.	1832	0951	15.25	23.16	1596	NE/E	C
6 Sept.	1832	1030	16.67	24.28	4277	NE	C
6 Sept.	1833	1234	20.28	26.75	3813	NE	C
6 Sept.	1833	1332	23.00	29.10	2364	N	C
7 Sept.	1834	0826	24.22	30.61	3496	SW	M/C
10 Sept.	1835	0644	24.31	27.30	3806	NW	C
10 Sept.	1835	0733	24.27	24.55	3792	NW	C
(b) Individual Smoke Plume Samples From Biomass Burning							
31 Aug.	1825	1136	20.97	34.69	225	–	P
31 Aug.	1825	1222	21.14	34.69	360	–	P
1 Sept.	1826	0920	14.78	24.45	1653	–	P
1 Sept.	1826	1004	14.78	24.45	1993	–	P
5 Sept.	1831	1212	14.80	24.49	1836	–	P
5 Sept.	1831	1224	14.79	24.48	1307	–	P
7 Sept.	1834	0859	24.36	31.25	644	–	P
7 Sept.	1834	0947	24.29	31.29	653	–	P
7 Sept.	1834	1037	24.15	30.97	540	–	P
(c) Ambient Air Samples in Namibia							
11 Sept.	1836	0910	22.90	13.10	3869	NW	M
11 Sept.	1836	1041	23.20	12.03	3104	NW	M
11 Sept.	1836	1059	23.50	12.70	3732	NW	M
13 Sept.	1837	1140	20.10	13.25	3908	E	C

[a]Local time = UTC + 2 hours.
[b]C, continental; M, maritime; M/C, mixed maritime and continental; P, individual biomass plume. Trajectories from *NOAA* [1997].

where $\beta(1)$ is determined from (2) and a humidograph of $\beta(1)$ versus RH.

5. Results and Discussion

5.1. Ambient Air Samples in South Africa, Mozambique, Botswana, and Zambia

[13] The curve fitting parameters for equations (1) and (2), and the derived values of $f(80\%, 550\text{ nm})$ and $f_{\beta(1)}(80\%, 550\text{ nm})$ based on the humidographs obtained in ambient air in South Africa, Mozambique, Botswana, and Zambia, are listed in Table 2a.

[14] Starting on 3 September 2000, there was a large decrease in visibility in southern African due to the transport of aged biomass smoke to the region from the north (H. Annegarn et al, "The River of Smoke:" Characteristics of the southern African springtime biomass burning haze, submitted to *Journal of Geophysical Research*, 2003). With

Table 2. Empirical Curve Fitting Parameters, Dry Scattering Coefficient, and Humidification Factors at a Wavelength of 550 nm[a]

Date (2000)	UW Flight Number	Time of Measurement,[b] UTC, hhmm	a	b	σ_{spd}, 10^{-6} m^{-1}	f (80%, 550 nm)	χ_r^2	c	d	$f_{\beta(1)}$ (80%, 550 nm)
(a) Ambient Air Samples in South Africa, Botswana, Mozambique and Zambia										
14 Aug.	1812	1312	3.82	6.10	39.08	1.97	39.12	−0.064	0.15	0.75
14 Aug.	1812	1337	2.63	1.39	37.93	1.96	33.66	−0.077	0.15	0.68
15 Aug.	1814	912	5.26	7.76	22.69	1.93	9.60	−0.007	0.12	0.97
17 Aug.	1815	826	1.95	5.47	18.56	1.57	25.14	−0.051	0.17	0.84
20 Aug.	1819	1151	3.69	1.14	39.89	2.00	11.09	−0.075	0.13	0.66
22 Aug.	1820	721	2.69	1.99	84.46	2.19	16.12	−0.066	0.12	0.66
22 Aug.	1820	951	2.17	3.50	56.12	1.93	4.82	−0.079	0.15	0.69
23 Aug.	1821	1227	1.79	2.21	75.00	1.86	6.26	−0.073	0.14	0.68
24 Aug.	1822	709	1.56	2.74	45.56	1.75	3.55	−0.071	0.14	0.71
24 Aug.	1822	945	2.23	2.41	26.97	2.05	2.25	−0.076	0.14	0.67
29 Aug.	1823	858	2.76	4.33	44.19	2.02	23.00	−0.110	0.17	0.61
29 Aug.	1823	928	2.70	3.79	36.25	2.10	13.65	−0.102	0.16	0.62
29 Aug.	1823	1005	2.38	4.21	33.64	1.90	12.37	−0.095	0.17	0.66
29 Aug.	1824	1317	1.42	3.09	38.07	1.66	23.82	−0.075	0.14	0.69
29 Aug.	1824	1337	2.14	3.29	35.55	1.95	19.68	−0.081	0.15	0.67
31 Aug.	1825	932	3.89	4.46	25.58	2.39	13.53	−0.104	0.17	0.64
31 Aug.	1825	1108	1.54	4.85	111.20	1.51	8.16	−0.082	0.18	0.73
1 Sept.	1826	612	2.73	3.90	20.55	2.09	2.14	−0.093	0.16	0.65
1 Sept.	1826	718	2.05	3.85	36.78	1.83	7.08	−0.109	0.19	0.65
1 Sept.	1826	802	1.39	4.93	82.12	1.46	1.07	−0.077	0.18	0.75
2 Sept.	1829	852	3.50	6.27	53.08	1.86	6.29	−0.099	0.18	0.66
2 Sept.	1829	1019	1.29	4.96	90.90	1.42	9.13	−0.073	0.17	0.76
3 Sept.	1830	733	1.29	3.79	92.49	1.53	1.55	−0.068	0.15	0.74
3 Sept.	1830	843	1.06	4.23	220.45	1.40	1.72	−0.060	0.15	0.77
3 Sept.	1830	1021	1.82	6.63	110.64	1.41	1.67	−0.063	0.15	0.76
3 Sept.	1830	1058	1.33	3.00	140.08	1.62	15.57	−0.061	0.14	0.75
3 Sept.	1830	1124	0.63	3.20	138.44	1.29	5.50	−0.067	0.14	0.73
5 Sept.	1831	910	1.96	6.45	117.75	1.46	2.83	−0.064	0.14	0.74
5 Sept.	1831	1005	1.10	3.52	144.94	1.48	2.60	−0.062	0.13	0.73
5 Sept.	1831	1040	1.15	3.06	190.10	1.54	3.98	−0.058	0.13	0.73
5 Sept.	1831	1245	1.17	4.77	143.27	1.40	5.03	−0.037	0.13	0.85
6 Sept.	1832	728	1.91	7.86	219.06	1.33	3.48	−0.047	0.12	0.78
6 Sept.	1832	755	0.86	6.53	234.04	1.20	1.57	−0.054	0.15	0.79
6 Sept.	1832	911	0.88	3.89	215.94	1.36	2.08	−0.055	0.15	0.79
6 Sept.	1832	951	1.19	4.90	207.49	1.40	22.96	−0.040	0.14	0.84
6 Sept.	1832	1030	1.15	3.97	186.11	1.46	3.10	−0.066	0.13	0.69
6 Sept.	1833	1234	1.59	3.36	115.81	1.70	21.23	−0.061	0.13	0.73
6 Sept.	1833	1332	1.23	2.47	106.09	1.61	17.33	−0.063	0.14	0.73
7 Sept.	1834	826	2.62	4.91	7.74	1.86	15.18	−0.090	0.16	0.66
10 Sept.	1835	644	1.59	4.98	73.76	1.52	3.82	−0.060	0.13	0.73
10 Sept.	1835	733	1.47	4.69	54.75	1.51	1.41	−0.055	0.13	0.76
(b) Individual Smoke Plume Samples From Biomass Burning										
31 Aug.	1825	1136	1.78	4.16	352.35	1.68	3.50	−0.069	0.23	0.83
31 Aug.	1825	1222	1.07	3.93	193.37	1.43	4.52	0.003	0.20	1.01
1 Sept.	1826	920	1.08	3.73	252.34	1.45	2.78	−0.024	0.18	0.93
1 Sept.	1826	1004	1.42	3.82	116.76	1.58	3.32	0.043	0.14	1.14
5 Sept.	1831	1212	1.88	5.96	261.14	1.49	2.07	0.006	0.16	1.02
5 Sept.	1831	1224	0.66	4.06	317.96	1.26	1.42	0.003	0.16	1.01
7 Sept.	1834	859	2.18	5.04	1093.79	1.70	4.16	−0.066	0.20	0.82
7 Sept.	1834	947	2.05	4.15	217.22	1.79	2.74	−0.038	0.20	0.90
7 Sept.	1834	1037	1.24	4.97	255.14	1.41	1.44	−0.076	0.20	0.78
(c) Ambient Air Samples in Namibia										
11 Sept.	1836	910	2.75	5.51	36.05	1.80	3.93	−0.052	0.11	0.74
11 Sept.	1836	1041	2.88	6.97	36.93	1.61	1.62	−0.036	0.10	0.80
11 Sept.	1836	1059	1.54	6.84	30.02	1.33	2.66	−0.038	0.10	0.79
13 Sept.	1837	1140	1.83	4.85	70.36	1.61	1.09	−0.066	0.14	0.73

[a]Listed are the fitting parameters a and b to equation (1) and c and d to equation (2), the dry scattering coefficient, σ_{spd}, and the humidification factors, f(80%, 550 nm) and $f_{\beta(1)}$(80%, 550 nm). χ_r^2 provides a measure of the dispersion of the fit of equation (1) to the humidograph. For locations of samples, see Table 1.

[b]Local time = UTC + 2 hours.

a few exceptions, we will refer to ambient air sampled between 14 August and 2 September 2000, as "ambient regional air samples"; ambient air sampled during the low-visibility period of 3–10 September 2000, with airflows from the northwest, north, and northeast of the sample location, will be referred to as "ambient aged heavy smoke samples." The exceptions to this general categorization are as follows. A humidograph obtained at 1108 UTC on 31 August was categorized as "ambient aged heavy smoke," since its σ_{spd} value was very high (Table 2a) and the most

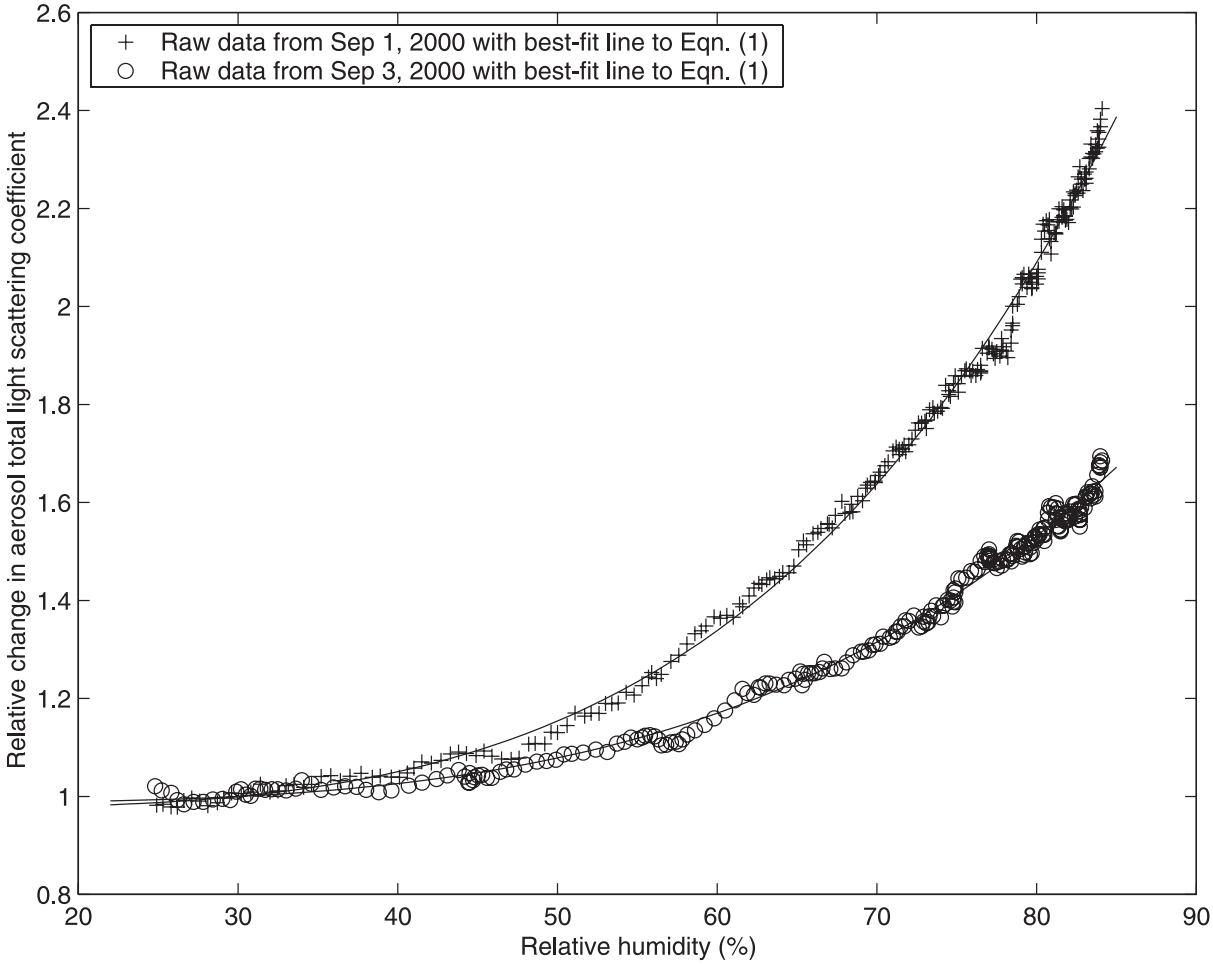

Figure 2. Humidographs obtained in northern South Africa of the aerosol total light scattering coefficient at 550 nm for an ambient regional air sample obtained at 0612 UTC on 1 September 2000, and for an ambient aged heavy smoke sample obtained at 0733 UTC on 3 September 2000. The humidograph for 1 September is characteristic of those obtained for regional ambient air samples from 14 August to 2 September 2000, and the humidograph for 3 September is characteristic of those obtained in ambient aged heavy smoke samples from 3 September to 10 September 2000, when the region was dominated by heavy smoke from the north. The lines are best fit curves to equation (1).

recent airflow was from the north (Table 1). Humidographs obtained at 0802 UTC on 1 September and 1019 UTC on 2 September were also classified as "ambient aged heavy smoke" because their σ_{spd} values were high (Table 2a) and the humidographs were obtained in tropical Zambia (Figure 1) which was dominated by smoke from biomass burning. Finally, on 7 September the airflow was from the southwest (Table 1a), therefore, this humidograph was classified as an "ambient regional air sample."

[15] Humidographs for a typical ambient regional air sample and a typical ambient aged heavy smoke sample, together with the corresponding best fit curves to equation (1), are shown in Figure 2. These two humidographs are quite different, although they were obtained at nearly identical locations in northeastern South Africa and just two days apart. However, the sample on 1 September shown in Figure 2 was in airflow from the southeast, and the sample on 3 September shown in Figure 2 was in airflow from the north-northwest, which transported heavy smoke from tropical Africa. As can be seen, the aerosol total light scattering coefficient for the ambient regional air sample on 1 September increases much more with increasing RH than that for the ambient aged heavy smoke sample on 3 September.

[16] The best fits to equation (1) for the aerosol total light scattering coefficient for all of the ambient regional air samples, and all of the ambient aged heavy smoke samples, are shown in Figure 3. Listed in Table 3 are the values of a, b, σ_{spd}, and f(80%, 550 nm) for the ambient regional air samples and for the ambient aged heavy smoke samples. It can be seen that both the fitting parameters and the humidification factors are significantly different for these two data sets. On average, the value of f(80%, 550 nm) for the ambient aged heavy smoke samples was 30% less than for the ambient regional air samples.

[17] The best fit curves to equation (2) for the aerosol hemispheric backscatter ratio for all of the ambient regional air samples, and all of the ambient aged heavy smoke samples, are shown in Figure 4. The values of the fitting parameters c and d and the humidification factor $f_{\beta(1)}$(80%,

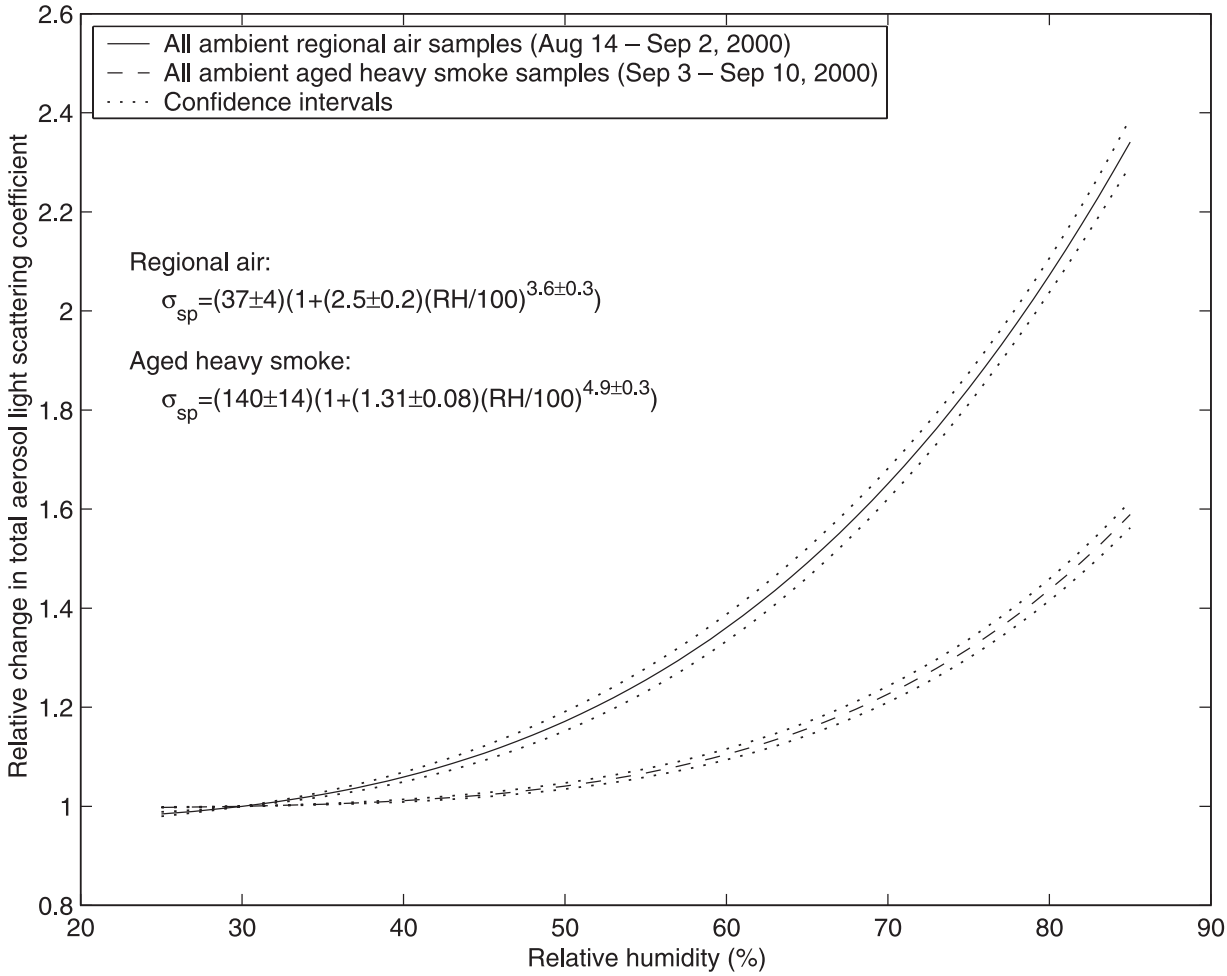

Figure 3. Best fit humidographs for the aerosol total light scattering coefficient at 550 nm for all of the ambient regional air samples from 14 August to 2 September 2000, and all of the ambient aged heavy smoke samples from 3 September to 10 September 2000. Dotted lines indicate confidence limits.

Table 3. Summary of Results for Ambient Air Samples and Individual Smoke Plume Samples From Biomass Fires[a]

	Number of Samples	f (80%, 550 nm)	a	b	σ_{spd}, 10^{-6} m^{-1}	$f_{\beta(1)}$ (80%, 550 nm)	c	d
All ambient air samples in South Africa, Mozambique, Botswana and Zambia (14 Aug. to 10 Sept. 2000)	41	1.59 ± 0.04	1.64 ± 0.12	4.53 ± 0.23	113 ± 11	0.72 ± 0.04	−0.067 ± 0.003	0.141 ± 0.003
Ambient regional air samples (14 Aug. to 2 Sept. 2000)	20	2.07 ± 0.03	2.55 ± 0.19	3.59 ± 0.33	37 ± 4	0.69 ± 0.05	−0.076 ± 0.005	0.147 ± 0.004
Ambient aged heavy smoke samples (3 Sept. to 10 Sept. 2000)	21	1.44 ± 0.02	1.31 ± 0.08	4.88 ± 0.28	140 ± 14	0.76 ± 0.04	−0.058 ± 0.002	0.136 ± 0.004
All individual smoke plume samples from biomass burning	9	1.50 ± 0.06	1.39 ± 0.18	4.50 ± 0.25	312 ± 76	0.93 ± 0.10	−0.023 ± 0.013	0.177 ± 0.009
Individual smoke plume samples from biomass burning collected within 10 min of emission	4	1.66 ± 0.08	1.73 ± 0.25	4.20 ± 0.26	427 ± 190	0.87 ± 0.08	−0.047 ± 0.010	0.193 ± 0.009
Individual smoke plume samples from biomass burning collected between 10 and 50 min of emission	5	1.42 ± 0.05	1.21 ± 0.21	4.66 ± 0.39	252 ± 31	0.99 ± 0.14	−0.004 ±0.019	0.164 ± 0.012
Ambient air samples in Namibia (11 Sept. to 16 Sept. 2000)	4	1.59 ± 0.07	2.19 ± 0.32	5.88 ± 0.57	50 ± 10	0.76 ± 0.13	−0.046 ± 0.007	0.110 ± 0.009

[a]Listed are the humidification factors for the aerosol total light scattering coefficient and the aerosol hemispheric backscatter ratio, and the fitting parameters a, b, and σ_{spd} for equation (1) and c and d for equation (2) at a wavelength of 550 nm.

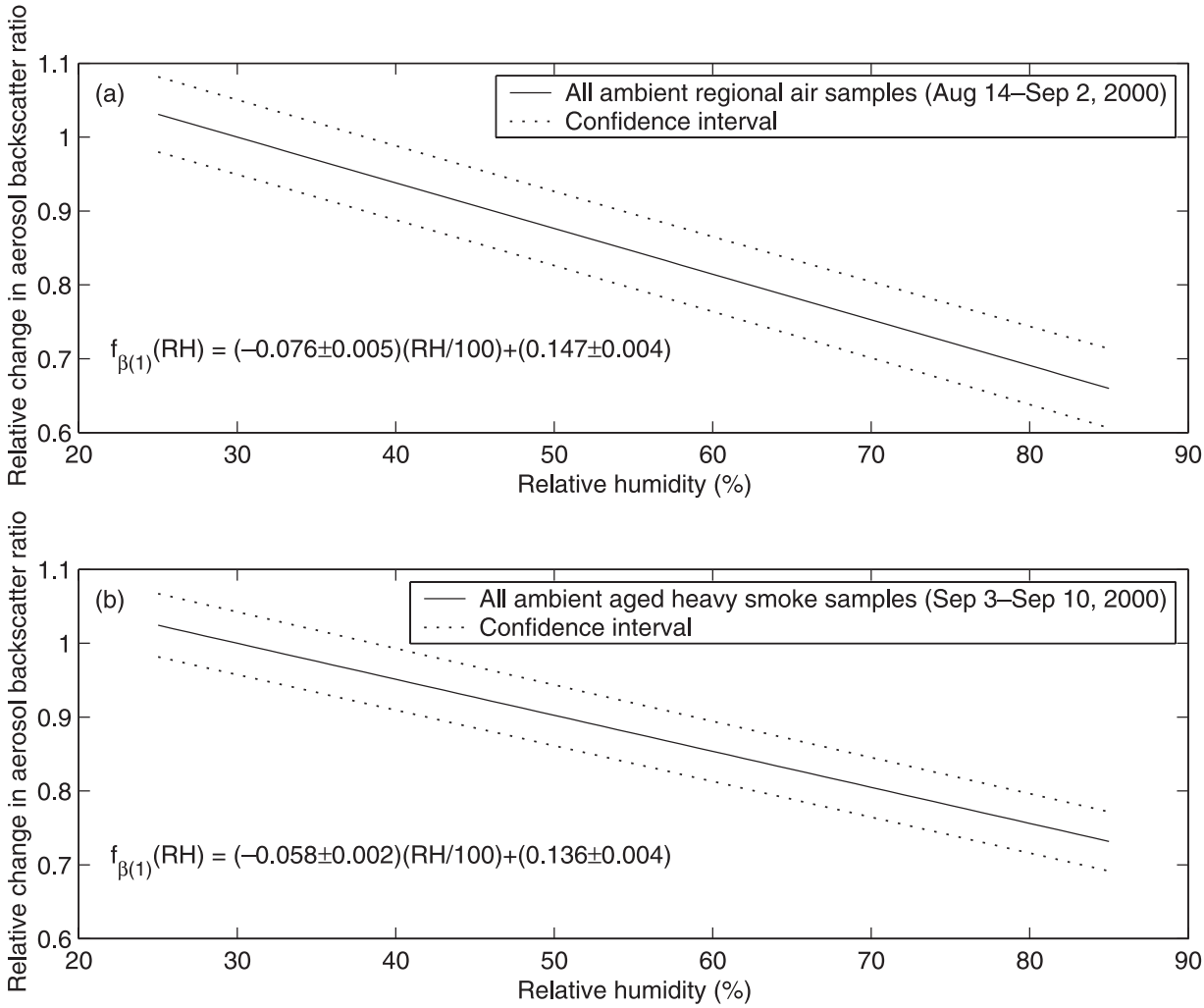

Figure 4. (a) Humidographs for the aerosol hemispheric backscatter ratio at a wavelength of 550 nm for all of the ambient regional air samples from 14 August to 2 September 2000. Dotted lines show confidence interval. (b) Humidographs for the aerosol hemispheric backscatter ratio at a wavelength of 550 nm for all of the ambient heavy smoke samples from 3 September to 10 September 2000. Dotted lines indicate confidence limits.

550 nm) are given in Table 3. In this case, $f_{\beta(1)}$(80%, 550 nm) was 10% larger for the aerosol perturbed by aged heavy smoke from tropical Africa than it was for the ambient regional air samples.

5.2. Individual Smoke Plumes From Biomass Burning

[18] Nine useable humidographs were obtained in individual smoke plumes from biomass fires in South Africa, Botswana, Mozambique, and Zambia. Information on these humidographs is given in Tables 1b and 2b, and the average values of the fitting parameters to equations (1) and (2) are given in Table 3.

[19] Smoke plumes from some of the biomass fires were intercepted at various distances downwind of the fires to compare the properties of very young smoke with those of somewhat aged smoke. A large 1000-hectare prescribed fire in the Timbavati Game Reserve in South Africa on 7 September 2000 [*Hobbs et al.*, 2003] provided the most comprehensive data of this type. Humidographs obtained in smoke samples that were 4 min and 45 min old in the plume from the Timbavati fire are shown in Figure 5. The age of the smoke was determined by wind speeds and the position of the aircraft with respect to the fire, both of which were measured aboard the aircraft. As the smoke aged over a period of ~40 min, and mixed with the ambient air, the humidification factor f(80%, 550 nm) decreased from about 1.7 to 1.41 (Figure 5 and Table 2b).

[20] Figures 6 and 7 show the effects of smoke aging on f(80%, 550 nm) and $f_{\beta(1)}$(80%, 550 nm), respectively, utilizing data from all of the biomass fires we studied in SAFARI 2000. Comparisons of Figures 3 and 6, and inspection of Table 3, show that after 10–50 min of aging and mixing with the ambient air, smoke from individual biomass fires had similar humidographs and f(80%, 550 nm) values to the much older ambient aged heavy smoke sampled from 3–10 September 2000. As seen in Table 3, the average value of the humidification factor for the total light scattering coefficient for the individual smoke plume samples collected between 10–50 min of emission (1.42 ± 0.05) is not significantly different from the corresponding

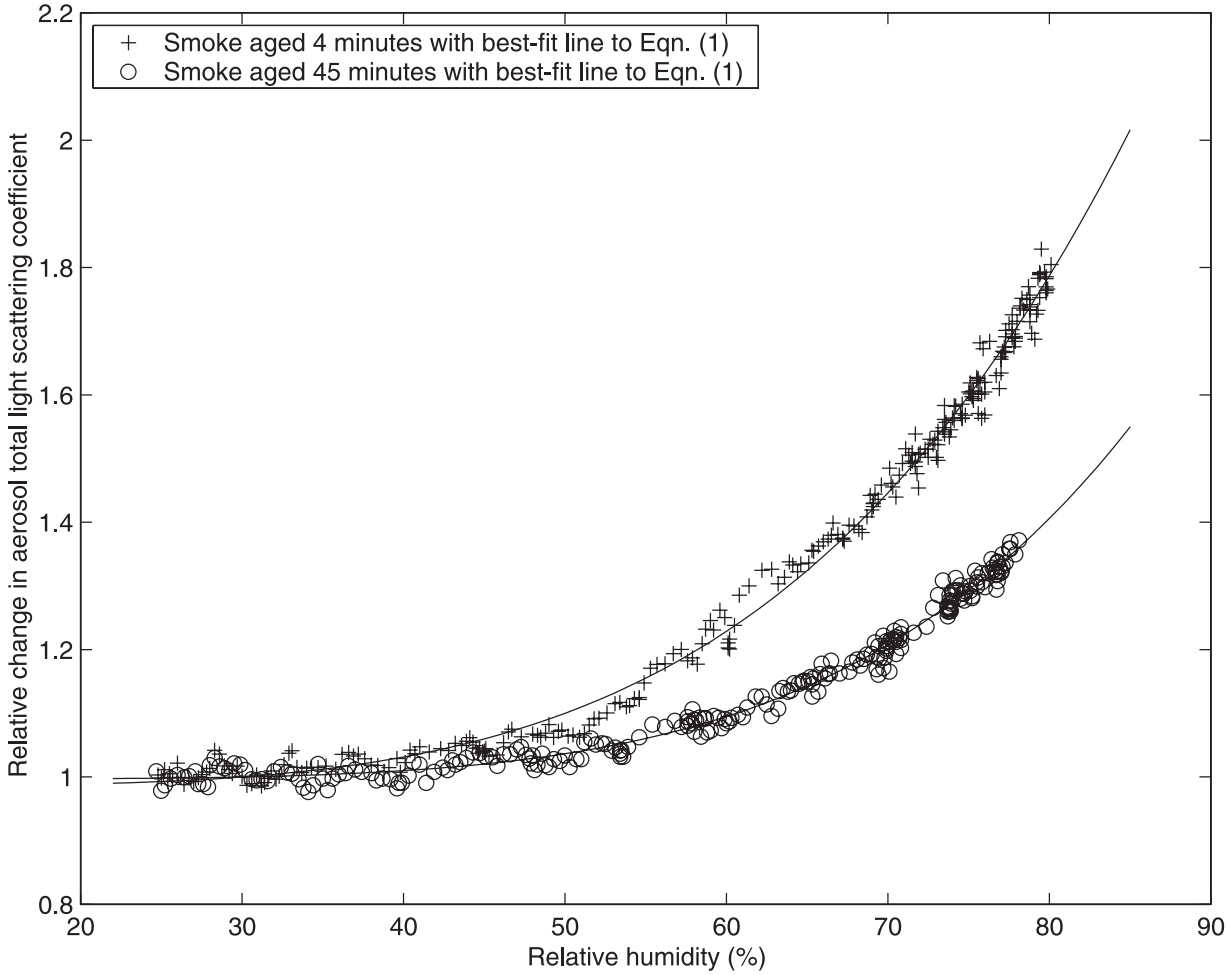

Figure 5. Humidographs at a wavelength of 550 nm for smoke samples from the Timbavati fires on 7 September 2000, showing the effect of smoke aging. The sample at 4 min downwind was obtained at 0947 UTC, and the sample at 45 min downwind at 1037 UTC.

value for the ambient aged heavy smoke samples (1.44 ± 0.02). Thus, as far as the effect of humidity on f(80%, 550 nm) is concerned, the effects of the aging of smoke and its mixing with the ambient air are essentially realized within less than an hour. A comparison of Figures 4 and 7 reveals that the $f_{\beta(1)}$(80%, 550 nm) values measured in smoke samples 10- to 50-min old are between 14% and 15% greater than the $f_{\beta(1)}$(80%, 550 nm) values measured in the ambient aged much older heavy smoke samples.

[21] *Pósfai et al.* [2003] and *Li et al.* [2003] describe the aerosol emitted from biomass fires in southern Africa based on individual particle analysis using electron microscopy. Pósfai et al. found that hydrophobic "tar balls" were more common in aged smoke. Li et al. suggest that the rapid conversion of KCl in young smoke to K_2SO_4 and KNO_3 in aged smoke reduces the hygroscopicity of the smoke particles. These suggestions are consistent with our observations of lower humidification factors in recently aged smoke.

5.3. Ambient Air Samples in Namibia

[22] Three humidographs were obtained just off the coast of Namibia on 11 September 2000, and one humidograph was obtained on the northern coast of Namibia on 13 September 2000 (Tables 1c and 2c). These humidographs did not differ significantly from each other. Seventy-two-hour and 120-hour model back trajectories [*National Oceanic and Atmospheric Administration* (*NOAA*), 1997] show that on 11 September the airflow was from tropical Africa, which presumably transported aged smoke to Namibia. On 13 September the airflow was from the east, which is also a source of biomass smoke.

[23] As shown in Table 3, the average value of f(80%, 550 nm) for the Namibian samples was 1.59 ± 0.07, compared to 1.59 ± 0.04 for all of the ambient air samples in South Africa, Mozambique, Botswana and Zambia. Thus, as far as the humidification factor for σ_{sp} is concerned, the few humidographs obtained in Namibia were identical to those obtained in South Africa, Mozambique, Botswana and Zambia. Similarly, the humidification factors for $\beta(1)$ for these two general locations were very similar.

5.4. Wavelength Dependence of Humidification Factors

[24] So far we have confined our discussions to the effects of relative humidity on light scattering by particles

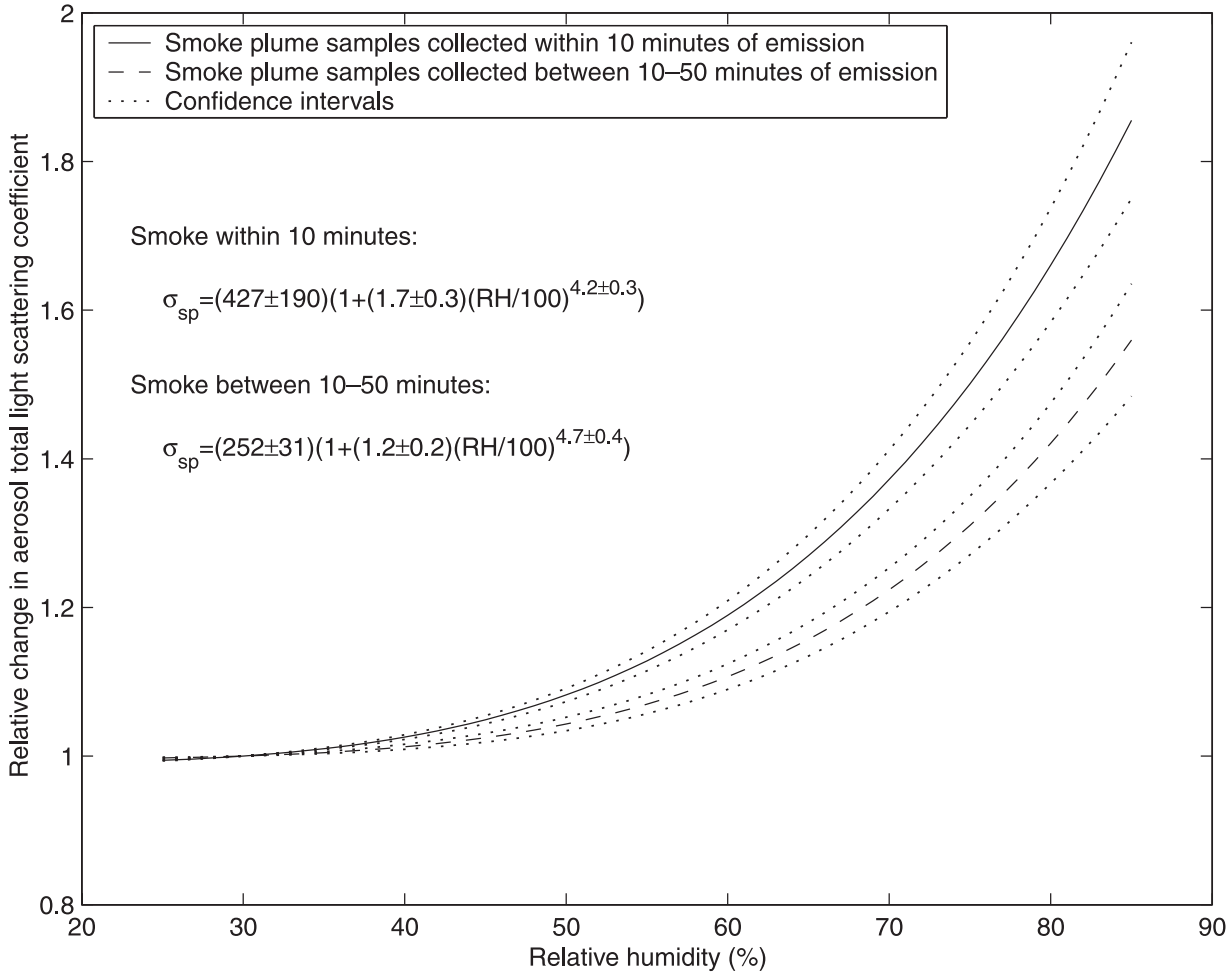

Figure 6. Best fit curves to equation (1) for humidographs at a wavelength of 550 nm for all smoke samples emitted within ~10 min and within ~10–50 min of emission from individual biomass fires. Dotted lines indicate confidence limits.

at a wavelength of 550 nm. However, simultaneous measurements were made at wavelengths of 450 and 700 nm. To determine if the humidification factors varied significantly with wavelength, we used the analysis of variance (ANOVA) test on the data. Given a set of sample populations, the ANOVA test gives the probability that the populations are independent [*Bevington and Robinson*, 1992].

[25] The ANOVA test showed that for the ambient regional air samples in South Africa, Botswana, Mozambique, and Namibia there was an 89% chance that $f(80\%, \lambda)$ was wavelength dependent, and an 54% chance that $f_{\beta(1)}(80\%, \lambda)$ was wavelength dependent. The values of $f(80\%, \lambda)$ for the ambient regional air samples increased by an average of 6% when the wavelength increased from 450 to 750 nm, and $f_{\beta(1)}(80\%, \lambda)$ decreased by 4% over the same wavelength interval. For ambient aged heavy smoke samples, there was a 7% chance that $f(80\%, \lambda)$ was wavelength dependent, and a 74% chance that $f_{\beta(1)}(80\%, \lambda)$ was wavelength dependent. The values of $f(80\%, \lambda)$ increased by 7%, and $f_{\beta(1)}(80\%, \lambda)$ decreased by 4%, when the wavelength was increased from 450 to 750 nm.

[26] For a change in wavelength from 450 to 750 nm, $f(80\%, \lambda)$ for the individual smoke plume samples increased monotonically by 8% for smoke sampled immediately above the fires and for smoke ~40 min old. For this same change in wavelength, $f_{\beta(1)}(80\%, \lambda)$ increased by 3% for the very young smoke and by 1% for smoke ~40 min old.

5.5. Altitude Dependence of Humidification Factor

[27] The humidification factors for both the ambient regional air samples and the ambient aged heavy smoke samples showed minimal altitude dependence from 1 to 4 km (Figure 8). For example, $f(80\%, 550\text{ nm})$ for the ambient regional air samples increased by about 4%, and $f(80\%, 550\text{ nm})$ for the ambient aged heavy smoke samples increased by about 10%, as the altitude increased from 1 to 4 km. Similar results applied to humidification factors at wavelengths of 450 and 700 nm.

5.6. Uncertainties in Humidification Factors

[28] The uncertainty in the values of $f(80\%, 550\text{ nm})$ listed in Table 3 were determined by finding the fitting parameters for each humidograph based on equation (1) and then calculating a χ_r^2 weighted average set of fitting

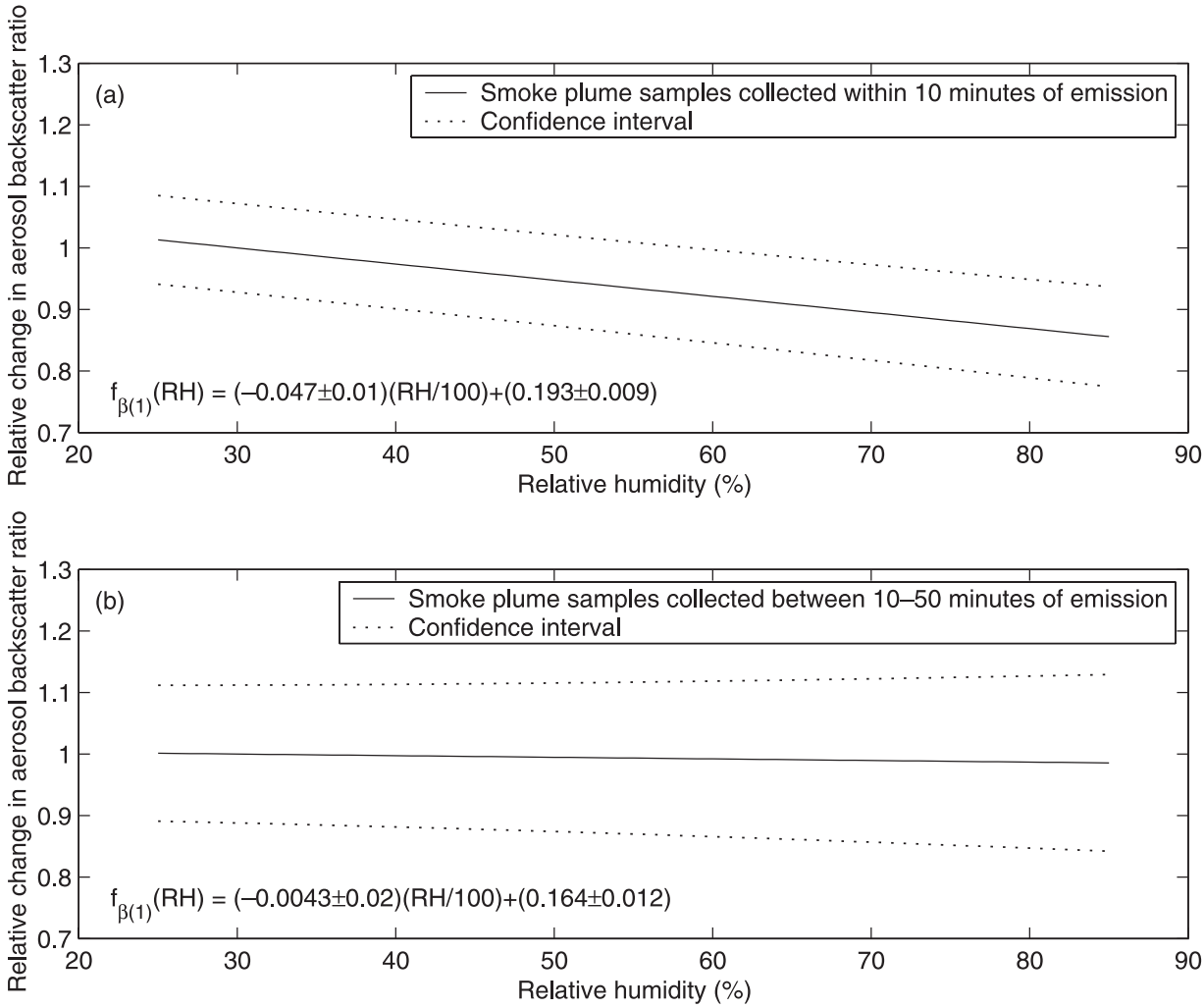

Figure 7. Best fit curves to equation (2) for the hemispherical backscatter ratios at a wavelength of 550 nm for (a) smoke samples collected within ~10 min and (b) smoke samples collected within ~10–50 min of emissions from individual fires. Dotted line indicates confidence limits.

parameters for each category. For example, the ambient aged heavy smoke samples consist of 21 humidographs (and thus 21 individual χ_r^2 parameters). Therefore, the fitting parameters describing the best fit curve to these data are the χ_r^2 weighted averages of 21 parameters. These χ_r^2 weighted fitting parameters were used to calculate the f(80%, 550 nm) values listed in Table 3. The uncertainty in f(80%, 550 nm) was determined by calculating f(80%, 550 nm) for each of the humidographs and finding the uncertainty in the χ_r^2 weighted average value. The values of χ_r^2 for the humidographs used in this study are listed in Table 2.

[29] The uncertainties in the $f_{\beta(1)}$(80%, 550 nm) values listed in Table 3 were determined by propagating the uncertainty in the mean value of each of the fitting parameters through equation (2) to arrive at a calculated mean $f_{\beta(1)}$(80%, 550 nm) with associated uncertainty. The errors associated with the fitting parameters from each humidograph were negligible, and are therefore not listed in Table 2. We use only the scatter of the fitting parameters about their means.

6. Summary and Conclusions

[30] From an analysis of 54 humidographs (i.e., aerosol total light scattering coefficient, σ_{sp}, or aerosol hemispheric backscatter ratio, $\beta(1)$, versus relative humidity, RH) obtained in five countries in southern Africa during the dry biomass burning season, the following principal results have been obtained.

1. The humidographs for both the ambient aerosols and those in individual smoke plumes from biomass burning could be fitted to expressions of the form:

$$\sigma_{sp} = \sigma_{spd}\left[1 + a\left(\frac{RH}{100}\right)^b\right]$$

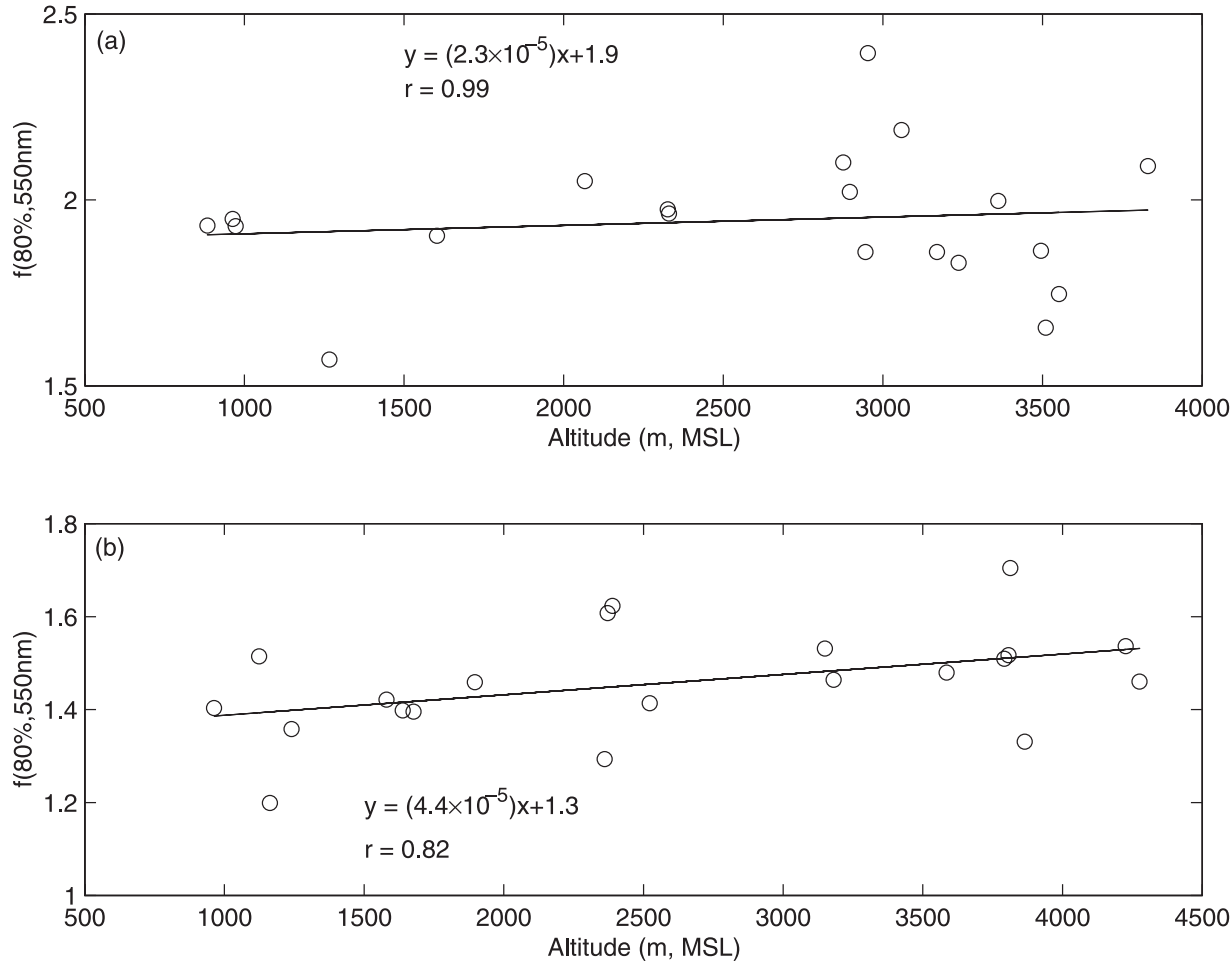

Figure 8. Altitude dependence of f(80%, 550 nm) at a wavelength of 550 nm for (a) ambient regional air samples and (b) ambient aged heavy smoke samples. Best fit lines and equations to the data are shown.

and,

$$\beta(1) = c\left(\frac{RH}{100}\right) + d$$

2. Values of the fitting parameters a, b, σ_{spd}, c and d for the various aerosol are given in Tables 2 and 3.

3. When aged heavy smoke from tropical Africa was transported to the sample location, the increase of σ_{sp} with increasing RH was reduced. For example, at a wavelength of 550 nm, the ratio of σ_{sp} at an RH of 80% to σ_{sp} at an RH of 30% (called the humidification factor) was 30% less for the ambient aged heavy smoke samples than for ambient regional air samples at the same general locations.

4. The humidification factors for smoke in individual plumes from biomass fires that had aged for about 50 min were similar to those for the ambient aged heavy smoke samples from tropical Africa that had aged for several days.

5. Compared to the ambient regional air samples, the humidification factor for $\beta(1)$ was 10% larger when the ambient aerosol was perturbed by aged heavy smoke from tropical Africa.

6. The humidification factor for σ_{sp} for the ambient regional air samples increased by ~6% when the wavelength changed from 450 to 750 nm. For the same samples, the humidification factor for $\beta(1)$ decreased by ~4% when the wavelength changed from 450 to 750 nm.

[31] **Acknowledgments.** This research was supported by grants NAG5-9022 and NAG5-7675 from NASA's Radiation Science Program and grant ATM-9901624 from NSF's Division of Atmospheric Sciences. This study is part of the SAFARI 2000 Southern African Regional Science Initiative.

References

Bevington, P. R., and D. K. Robinson, *Data Reduction and Error Analysis for the Physical Sciences*, 2nd ed., McGraw-Hill, New York, 1992.

Hartley, W. S., and P. V. Hobbs, An aerosol model and aerosol-induced changes in the clear-sky albedo off the east coast of the United States, *J. Geophys. Res.*, *106*, 9733–9748, 2001.

Hartley, W. S., P. V. Hobbs, J. L. Ross, P. B. Russell, and J. M. Livingston, Properties of aerosols aloft relevant to direct radiative forcing off the mid-Atlantic coast of the United States, *J. Geophys. Res.*, *105*, 9859–9885, 2000.

Hegg, D. A., D. S. Covert, M. J. Rood, and P. V. Hobbs, Measurements of aerosol optical properties in marine air, *J. Geophys. Res.*, *101*, 12,893–12,903, 1996.

Hobbs, P. V., P. Sinha, R. J. Yokelson, T. J. Christian, D. R. Blake, S. Gao, T. W. Kirchstetter, T. Novakov, and P. Pilewskie, Evolution of gases and particles from a savanna fire in South Africa, *J. Geophys. Res.*, *108*(D13), 8485, doi:10.1029/2002JD002352, 2003.

Kasten, F., Visibility in the phase of pre-condensation, *Tellus*, *21*, 631–635, 1969.

Kotchenruther, R. A., and P. V. Hobbs, Humidification factors of aerosols from biomass burning in Brazil, *J. Geophys. Res.*, *103*, 32,801–32,089, 1998.

Kotchenruther, R. A., P. V. Hobbs, and D. A. Hegg, Humidification factors for atmospheric aerosols off the mid-Atlantic coast of the United States, *J. Geophys. Res.*, *104*, 2239–2251, 1999.

Li, J., M. Pósfai, P. V. Hobbs, and P. R. Buseck, Individual aerosol particles from biomass burning in southern Africa, 2, Compositions and aging of inorganic particles, *J. Geophys. Res.*, *108*(D13), 8484, doi:10.1029/2002JD002310, 2003.

National Oceanic and Atmospheric Administration (NOAA), HYSPLIT4 (Hybrid Single-Particle Langrangian Integrated Trajectory) Model, NOAA Air Resour. Lab., Silver Spring, Md., 1997. (Available at http://www.arl.noaa.gov/ready/hysplit4.html.)

Pilinis, C., S. N. Pandis, and J. H. Seinfeld, Sensitivity of direct climate forcing by atmospheric aerosols to aerosol size and composition, *J. Geophys. Res.*, *100*, 18,739–18,754, 1995.

Pósfai, M., R. Simonics, J. Li, P. V. Hobbs, and P. R. Buseck, Individual aerosol particles from biomass burning in southern Africa, 1, Compositions and size distributions of carbonaceous particles, *J. Geophys. Res.*, *108*(D13), 8483, doi:10.1029/2002JD002291, 2003.

Sinha, P., P. V. Hobbs, R. J. Yokelson, I. T. Bertschi, D. R. Blake, I. J. Simpson, S. Gao, T. W. Kirchstetter, and T. Novakov, Emissions of gases and particles from a savanna fire in South Africa, *J. Geophys. Res.*, *108*, doi:10.1029/2002JD002325, in press, 2003.

Wiscombe, W. J., and G. W. Grams, The backscattered fraction in two-stream approximations, *J. Atmos. Sci.*, *33*, 2440–2451, 1976.

P. V. Hobbs and B. I. Magi, Department of Atmospheric Sciences, University of Washington, Box 351640, Seattle, WA 98195-1640, USA. (phobbs@atmos.washington.edu; magi@atmos.washington.edu)